Progress In Electromagnetics Research M, Vol. 92, 43–54, 2020

Diagonally Asymmetric CSRRs Loaded Circularly Polarized Antenna with Frequency Selective Surface

Soumik Dey[1], Ankita Indu[2, *], Santanu Mondal[3], and Partha P. Sarkar[4]

Abstract—This paper presents a compact single feed circularly polarized (CP) antenna along with a frequency selective surface (FSS) that acts as a partially reflective surface over the patch. Patch is loaded with four diagonally asymmetric complementary split ring resonators (CSRRs) in order to achieve circular polarization. In this paper a novel design of reflective type FSS layer is presented at 2.4 GHz. The size of FSS unit cell is approximately $0.132\lambda_0 \times 0.132\lambda_0$, and it is placed at a distance of $0.146\lambda_0$ from the patch. Simulated impedance bandwidth of the antenna for $S_{11} < -10$ dB is from 2.385 to 2.506 GHz (121 MHz or 4.95%) which covers the entire IEEE 802.11 WLAN band (2.4–2.484 GHz). Position of the four CSRRs on the patch and the height of FSS screen are determined through parametric studies, and the detailed analyses in terms of reflection coefficient, axial ratio, and gain variation are also presented. Gain of the antenna is 3.02 dBic at the operating frequency 2.45 GHz. Measured results are in good agreement with the simulated ones.

1. INTRODUCTION

Ability to reduce the effect of multipath fading and polarization mismatch between transmitting and receiving antennas gives circularly polarized antennas adding advantage over linearly polarized antennas. In modern wireless devices, single feed technique is mostly used to obtain circular polarization instead of dual-feed CP antenna in order to achieve compactness and avoid complexity in feeding network [1, 2]. The slot of different geometries like rectangle, cross, or Y-shape is etched on the radiating patch to perturb the current distribution in order to excite two degenerate modes [3–5]. Another common method to design single feed CP antenna is perturbing the boundary of the patch by being loaded with either a pair of stubs, notches on the opposite edges [6] or truncating diagonally opposite corners of the patch [7]. In recent years, microstrip antenna loaded with combination of asymmetric circular slots along diagonal directions having different radii and additional symmetric orthogonal slits has been proposed for circularly polarized operation by Nasimuddin et al. [8]. In [9], the same work has been extended for square, cross, and square ring shape slots, and design technique has been reported in detail. Compactness in single feed CP antenna has been realized by cutting four V-shaped asymmetric slits on the patch along diagonal directions [10]. Recently, metamaterial structures are getting much attention for antenna size reduction due to their unique properties of dual negative permittivity and permeability [11]. Commonly known resonating meta-structures are split ring resonator (SRR) and its dual complementary split ring resonator (CSRR). CSRR-loaded compact circularly polarized microstrip antennas have been proposed in [12–14]. In [15, 16], CSRRs are loaded on the patch and the ground plane of the microstrip antennas separately to obtain circular polarization. In [13, 16, 17], reactive impedance surface (RIS) has been combined between the radiating patch and ground plane to improve

Received 2 March 2020, Accepted 14 April 2020, Scheduled 5 May 2020

* Corresponding author: Ankita Indu (nkitaindu@gmail.com).

[1] Indian Institute of Technology, Palakkad. [2] B. P. Poddar Institute of Management and Technology, MAKAUT, India. [3] Institute of Radio Physics & Electronics, University of Calcutta, Kolkata, India. [4] Department of Engineering and Technological Studies, University of Kalyani, Kalyani, India.

the impedance bandwidth and radiation properties of the antenna at the expense of more design complexity and increase in the overall profile of the antenna.

In this article, the technique used in [9] is utilized to achieve circular polarization. However, in this work instead of commonly known slots geometries, four asymmetric CSRRs are diagonally placed over the patch to excite CP. It is observed that CSRRs loaded patch resonates at much lower frequency than the conventional geometrical shaped slotted patch, and hence miniaturization over the conventional antenna has been obtained. Low radiation efficiency and gain of the CSRRs loaded CP antenna have been improved by using FSS as a superstrate above the patch. Here a novel FSS unit cell having a fan-shaped slot on a square patch with a transmission zero at the operating frequency of the CP antenna is used as highly reflective surface. FSS is a kind of spatial filter that either transmits or reflects the electromagnetic waves over its operating frequency range. Besides the gain improvement of the microstrip antenna FSS can also be used as a planar vortex beam generator capable of generating orbital angular momentum under CP incidence [18]. The principle behind the gain improvement in this composite structure has been explained in [19] by simple ray tracing method of multiple reflections between the ground plane of antenna and superstrate layer, which is similar to Fabry-Perot Cavity resonator antenna (FP-CRA). Circular polarization in FP-CRA can be obtained either by using FSS as a polarization rotator over a linearly polarized antenna which is tilted by 45° [20] or by using FSS directly above a CP antenna [21]. In this paper, a compact CP antenna having asymmetrically loaded CSRRs along the diagonal direction is presented. The simulated results are computed using CST Microwave studio14 [23].

The design of the proposed CP antenna and FSS unit cell in detail are discussed in Sections 2–4, respectively. The characteristics of the antenna without and with FSS superstrate are compared in Section 5. Measured results are shown in Section 6, and finally conclusions are drawn in Section 7.

2. ANTENNA DESIGN

Geometry of the proposed CP antenna is shown in Fig. 1. Four asymmetric CSRRs are placed in diagonal directions of a nearly square patch with probe feed placed along the X-axis. The antenna is designed on a low cost FR4 substrate with dielectric constant 4.3 and loss tangent 0.025. The overall antenna dimension is $(50 \times 50 \times 1.6)\,\text{mm}^3$, and the patch size is $25.6\,\text{mm} \times 25.2\,\text{mm}$ $(0.205\lambda_0 \times 0.202\lambda_0)$ at 2.4 GHz. L_p and W_p are the patch length and width along X and Y axes, respectively.

The centres of the four CSRRs are located at (P, P), $(P, -P)$, $(-P, -P)$, and $(-P, P)$ where

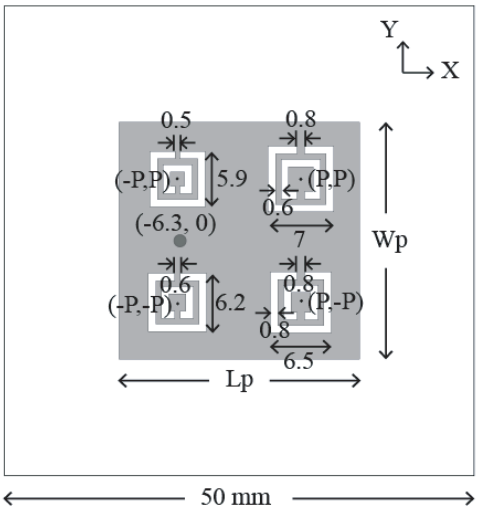

Figure 1. Geometry of the asymmetric CSRRs loaded CP antenna: $Lp = 25.6\,\text{mm}$, $Wp = 25.2\,\text{mm}$ and $P = 6.56\,\text{mm}$.

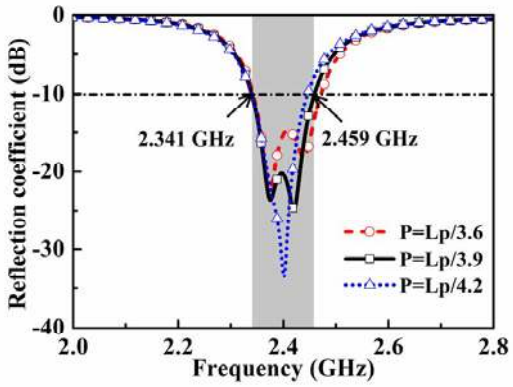

Figure 2. Reflection coefficient characteristics of the antenna for different positions of CSRRs.

$P = L_p/3.9$ and the perimeters of the outer rings of these four CSRRs are respectively C1, C2, C3, and C4. For obtaining circular polarization, the dimensions of the CSRRs are chosen in such a way that C1 > C2 > C3 > C4 is maintained. The probe feed is shifted 6.3 mm from the centre on the X axis to obtain 50 Ohm impedance matching. Ring splits of all CSRRs are along the Y axis which is orthogonal to the axis along which feed is placed. These particular orientations of ring splits are necessary to obtain circular polarization, and the reason has been explained in detail in [15]. Two orthogonal degenerate modes will be excited because of asymmetry along 45° to feed position. Feed location and positions of CSRRs are then adjusted to achieve 90° phase difference between the two modes with a good impedance matching at the operating frequency.

The reflection coefficient characteristics of the proposed CP antenna for three different positions of CSRRs (i.e., $P = L_P/3.6$, $L_P/3.9$ and $L_P/4.2$) with $L_P = 25.6$ mm and $W_P = 25.2$ mm are shown in Fig. 2. Different positions of CSRRs have major impacts on axial ratio plot as shown in Fig. 3. Also it is shown from Fig. 2 that lower resonance frequency of the two degenerated modes remains unchanged with the value of P. But higher resonance frequency shifts towards lower resonance frequency when the value of P is decreased, and hence operating bandwidth also decreases with decrease in value of P. Finally, for $P = L_P/4.2 = 6.09$ mm both modes resonate at the same frequency. For CSRRs' position at $P = L_P/3.9$ or 6.56 mm, the response for axial ratio and reflection coefficient are useful for ISM band applications. At this location of CSRRs, the simulated impedance bandwidth for $S_{11} < -10$ dB is 118.55 MHz (2.341–2.459 GHz) or 4.94% with centre frequency at 2.4 GHz. Minimum axial ratio is obtained at frequency 2.392 GHz and has the value 0.68 dB. The 3 dB axial ratio bandwidth for the antenna obtained in simulation is 28.26 MHz (2.379–2.407 GHz) or 1.18%. Gain variations of the antenna for these three CSRRs positions are shown in Fig. 4. It is clear that gain also significantly depends on the CSRRs relative positions.

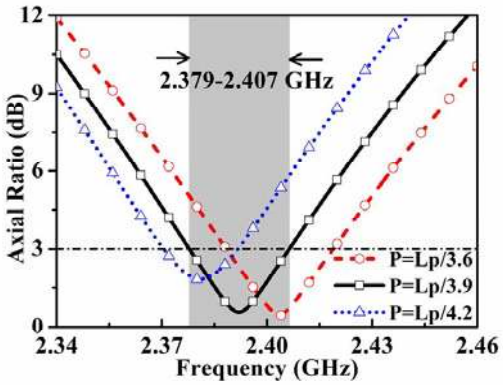

Figure 3. Axial ratio plot of the antenna for different positions of CSRRs.

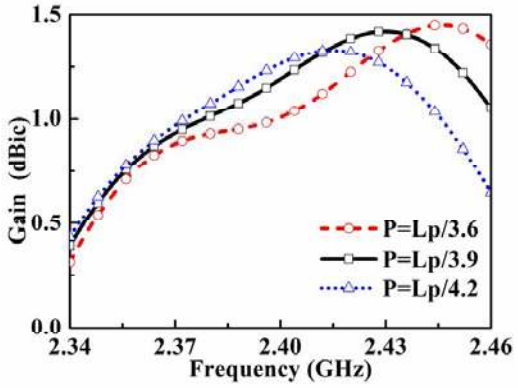

Figure 4. Gain plot of the antenna for different positions of CSRRs.

It is clear from Fig. 4 that the gain of the CSRRs loaded antenna is very low which can be attributed to the low radiation efficiency of the antenna. In this work to improve the gain of the antenna, frequency selective surface (FSS) is used as a superstrate above the patch radiating surface. Sections 4 and 5 describe design topology of the FSS and principle behind the gain improvement briefly.

3. COMPARISON WITH CONVENTIONAL SLOTS GEOMETRY

CSRR is a kind of meta resonating structure that poses the negative permittivity property and whose equivalent circuit model is a parallel L-C resonant tank circuit [11]. When a patch antenna is loaded with CSRR.

Due to additional inductive and capacitive loading patch resonance frequency will decrease. To further demonstrate this sub-resonance property of CSRR loaded patch, other traditional slots geometries are also loaded on the patch as in [8, 9]. Fig. 5(a) shows that patch antennas loaded with four asymmetric slots of circular, circular ring, square ring, and cross dipole shaped geometries.

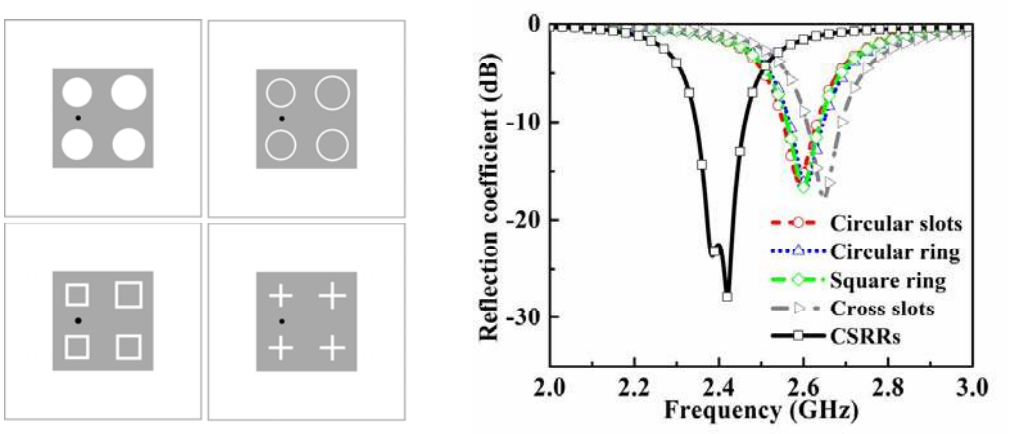

Figure 5. (a) Patches loaded with asymmetric circular, circular ring, square ring, cross dipole slots. (b) Reflection coefficient characteristics for antennas with different slots configuration.

For a fair comparison with the CSRRs loaded patch, the dimensions of the patches and ground planes in Fig. 5 are fixed to that of Fig. 1, and the positions, widths, and outer perimeters for all the slots geometries are made identical as discussed in Section 2. Reflection coefficients for patches with conventional geometrical shape slots along with CSRRs loaded patch are shown in Fig. 5(b) which clearly depicts that among all the situations, CSRRs loaded antenna resonates at much lower frequency.

4. FSS DESIGN

A novel bandstop FSS unit cell is designed at 2.4 GHz using the same substrate used for the antenna. Size of the FSS unit cell is 16.65 mm × 16.65 mm which is approximately $0.132\lambda_0 \times 0.132\lambda_0$, where λ_0 is the free space wavelength at frequency 2.4 GHz. Prototype of the FSS unit cell is shown in Fig. 6(a) which consists of four arms of a fan-shaped slot inside a square patch. FSS unit cell is simulated using CST microwave studio assuming periodic boundary condition and excited with a plane wave propagating along negative Z axis. Simulated reflection and transmission characteristics are presented in Fig. 6(b) for both TE and TM modes excitation which justifies the bandstop nature of this unit cell.

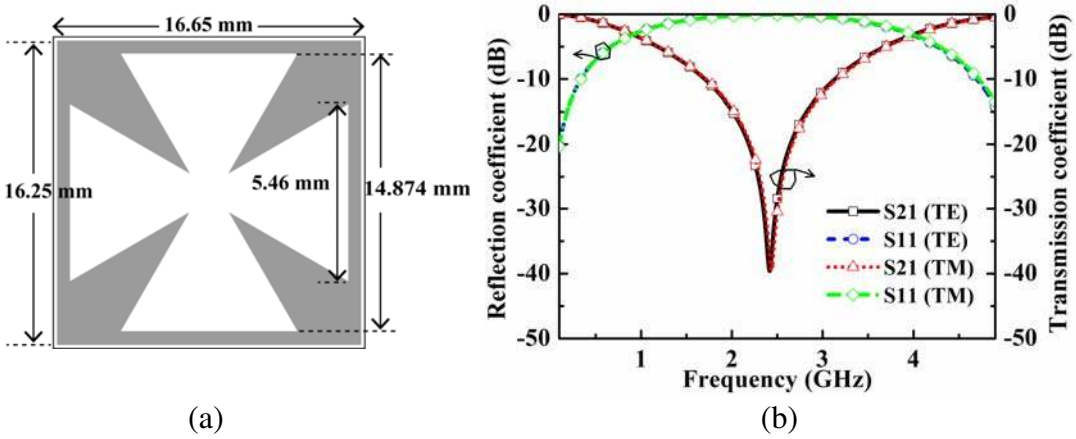

Figure 6. (a) Geometry of FSS unit cell and (b) its reflection and transmission response.

The FSS unit cell has zero transmission at 2.4 GHz, and simulated $S_{21} < -3$ dB bandwidths are 3.1 GHz (0.9–4 GHz). To get more physical insight for the proposed FSS surface current distribution is also shown in Fig. 7 for TE and TM modes at 2.4 GHz.

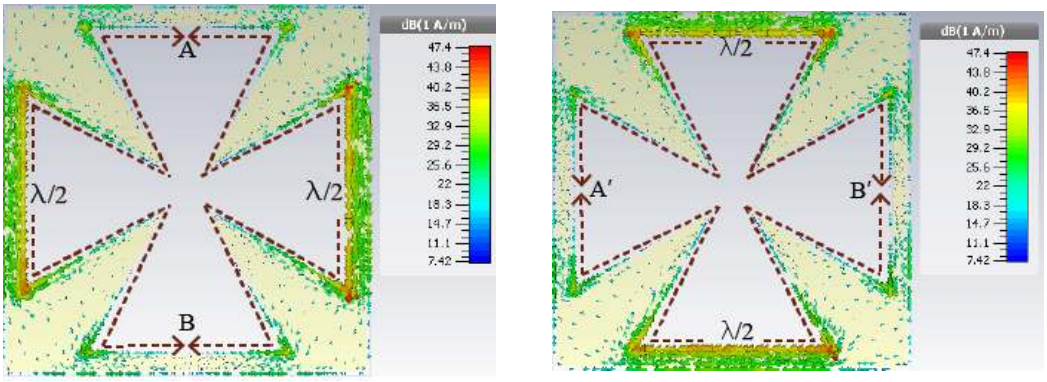

(a) (b)

Figure 7. Surface current distribution of proposed FSS for (a) TE and (b) TM modes.

Surface current distribution of this unit cell shows that at position A-B for TE mode and at A′-B′ for TM mode, the current directions have been changed, so the entire contour lengths A-B-A (TE) and A′-B′-A′ (TM) are approximately equal to one guided wavelength λ at the operating frequency. These extended current paths will increase the overall inductance of the unit cell. Two opposite arms of the fan-shaped slot where current is maximum contribute to the bandstop response, which is equivalent to a series L-C resonant circuit. The proposed unit cell has a fourfold symmetry which ensures a similar S-parameter response of the structure for different polarization angles of the incident wave as observed in Fig. 8.

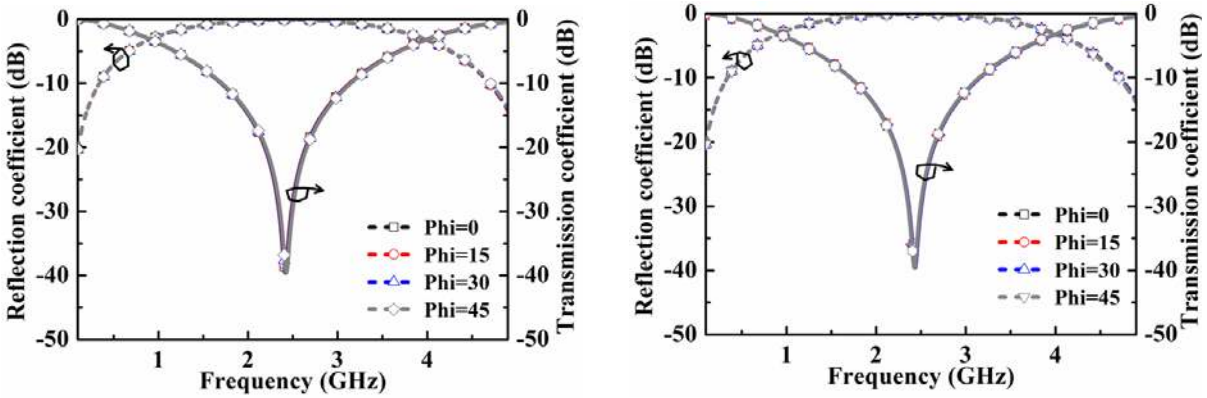

(a) (b)

Figure 8. Simulated S-parameter responses of the FSS for different polarization angle. (a) TE mode. (b) TM mode.

The FSS unit cell also shows good angular stability for both TE and TM modes for different incident angles of the wave with respect to normal. Fig. 9 shows that the designed FSS is angularly stable up to 60° with maximum frequency shift being 109 MHz (4.5%) for TE mode and 49 MHz (2%) for TM mode. Due to broadside radiation of the proposed CP antenna, such a small shift of resonance frequency for the FSS unit cell will practically have no effect.

Equivalent circuit of the unit cell is shown in Fig. 10(a). Under quasi-static analysis of microstrip line, the top FSS is modeled as a series R-L-C resonant circuit due to its bandstop characteristics. The substrate is modeled as a transmission line with a series inductance L_T and a shunt capacitance C_T. L_T and C_T are calculated by Telegrapher's Equations (1) and (2) [18, 22].

$$L_T = \mu_o \mu_r t \tag{1}$$

$$C_T = \varepsilon_o \varepsilon_r t \tag{2}$$

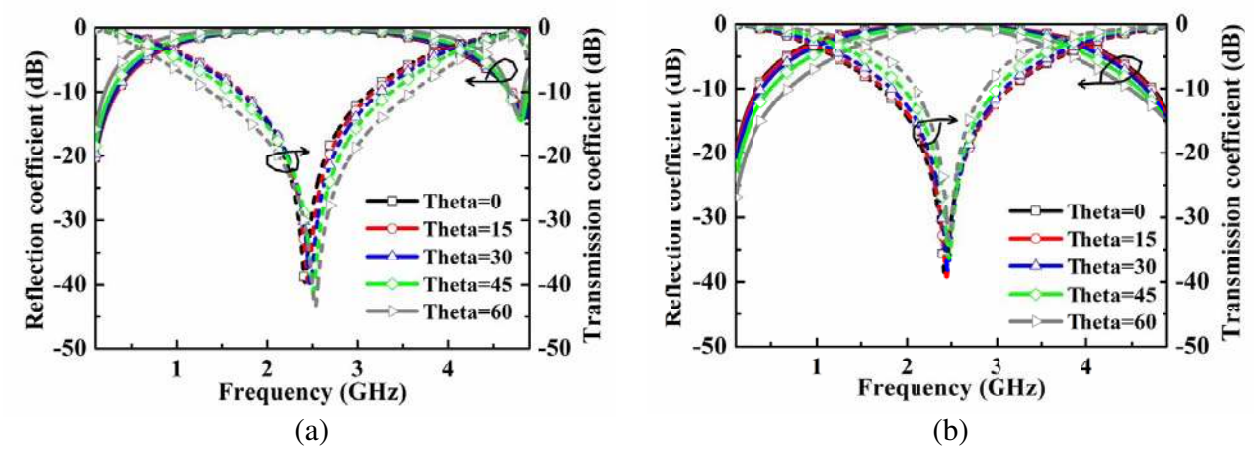

Figure 9. Simulated reflection and transmission responses for different incident angle. (a) TE mode. (b) TM mode.

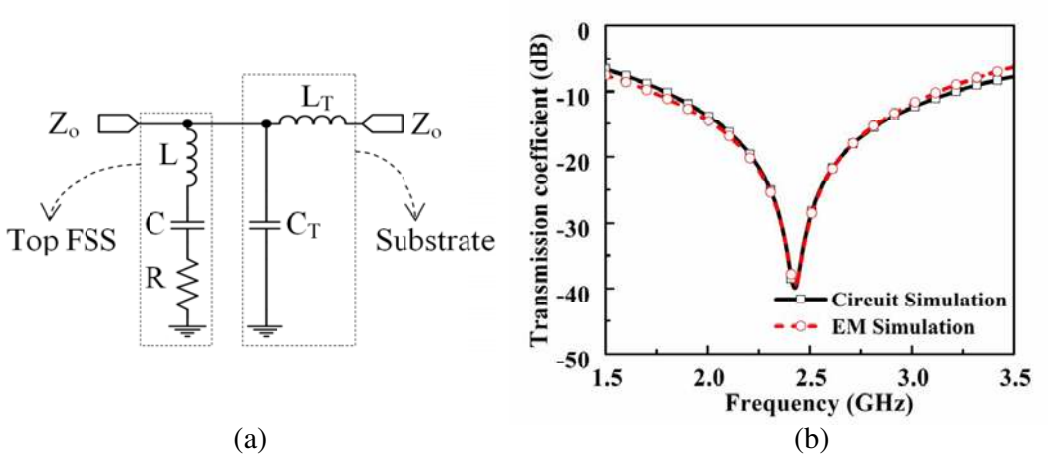

Figure 10. (a) Equivalent circuit of proposed unit cell. (b) Transmission coefficient of FSS in CST and ADS.

where $\varepsilon_o = 8.85 \times 10^{-12}$ F/m, $\mu_o = 4\pi \times 10^{-7}$ H/m, and ε_r, μ_r are relative permittivity and permeability of the substrate, $Z_o = 377\,\text{ohm}$, i.e., the free space impedance, and t is the thickness of the dielectric substrate.

L_T and C_T are calculated using the above equations. Values of L, R, C are obtained from circuit simulation using curve fitting technique. The circuit simulation results match well with the CST simulation results as shown in Fig. 10(b). The elements values are shown in the table below.

L_T	C_T	L	C	R
2 nH	62.3 fF	6.93 nH	0.621 pF	1.7 ohm

The input impedance (Z_{in}) of the unit cell is equal to the parallel combination of Z_{SUB} and Z_{FSS}, given in Equation (3), where $Z_{SUB} = L_T s + \frac{1}{C_T s}$, $Z_{FSS} = Ls + \frac{1}{Cs} + R$ with $s = j\omega$ and $Z_{in} = Z_{FSS} \| Z_{SUB}$.

$$Z_{in} = \frac{(LL_TCC_T)\,\omega^4 - j\,(L_TRCC_T)\,\omega^3 - (LC + L_TC_T)\,\omega^2 + j\omega\,(RC) + 1}{-j\omega^3\,(L_TC_TC + LCC_T) - \omega^2\,(RCC_T) + j\omega\,(C + C_T)} \tag{3}$$

5. ANTENNA WITH FSS

The proposed unit cell in the above section is used to form two-dimensional FSS screen which consists of 3×3 arrays placed at a height h from the ground plane of the patch. The relation among h, the reflection phases of FSS (Φ_{FSS}), ground plane (Φ_{GND}), and operating wavelength $\lambda(= c/f)$ is given by Equations (4) and (5) [18]

$$h = \frac{N\lambda}{2} + \frac{(\Phi_{FSS} + \Phi_{GND})\,\lambda}{4\pi}, \text{ where } N = 1, 2, 3 \ldots \tag{4}$$

$$\varphi_{GND} = \pi - 2\tan^{-1}\left[\tan(\beta d)/\sqrt{\varepsilon_r}\right] \tag{5}$$

where $\beta = 2\pi/\lambda$ represents the phase constant, and d is the antenna substrate thickness with dielectric constant ε_r. For the proposed FSS unit cell at 2.4 GHz, Φ_{FSS} is approximately $-179.3°$, and the reflection phase of the ground back antenna substrate is $\Phi_{GND} \sim 175.5°$. According to the above relation, h is found to be 61.8 mm which is approximately $\lambda/2$. But in this work through parametric optimization, the height of FSS superstrate above the antenna is determined near $\lambda/8$. So the proposed composite FSS loaded CP antenna also provides a low profile design. The prototype of the FSS loaded CP antenna is shown in Fig. 11. The simulated reflection coefficient characteristics of the antenna without and with FSS are shown in Fig. 12. From Fig. 12 it is observed that the resonant frequency of the composite FSS CP antenna shifts to higher frequency due to decrease in effective permittivity.

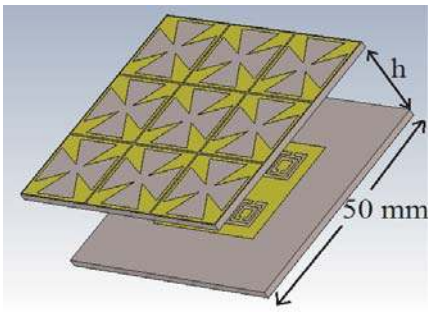

Figure 11. Configuration of composite CP antenna with FSS.

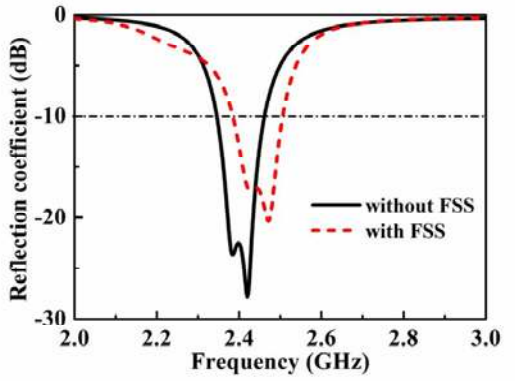

Figure 12. Simulated reflection coefficient of the antenna with and without FSS.

Parametric studies have been carried out to investigate the effect of the FSS superstrate height h above the radiating patch, on the simulated axial ratio and gain variation. The axial ratio and gain characteristics for different values of h are presented in Fig. 13 and Fig. 14, respectively. With height increase, the operating frequency of the antenna shifts to lower frequency due to the increasing height of the cavity.

From Fig. 13 and Fig. 14, it can be concluded that with height increase although better axial ratio values are obtained, the gain of the antenna decreases. So a compromise has to be made between gain and axial ratio while choosing appropriate height of the FSS screen. In this work, an optimized height of 18.3 mm is chosen for which gain is above 3 dBic, and axial ratio is below 2 dB. The gain of the composite antenna structure may be increased more by increasing the number of FSS array elements, but in this paper antenna size and FSS array size are assumed the same. Simulated axial ratios and gain variations of the antenna with and without FSS are shown in Fig. 15. From Fig. 15 it is shown that over the entire impedance bandwidth of the antenna, the minimum gain improvement is greater than 1.59 dBic. The shift in resonance frequency is observed in Fig. 15(a) due to variation in effective dielectric constant and also a change in input impedance of the antenna due to FSS loading.

In Table 1 the simulated impedance bandwidths for $S_{11} < -10$ dB, AR < 3 dB, gains, and radiation efficiencies of the CP antenna with and without FSS are presented.

The CP antenna gain can be further improved by increasing the array size for the FSS. Two different array sizes — 5×5 FSS with overall antenna size of 84 mm $\times$ 84 mm $\times$ 8.5 mm and 7×7 FSS with overall

antenna size of 117 mm × 117 mm × 9.1 mm — are used to compare the respective antenna performances with that of the antenna with 3 × 3 FSS. Fig. 16 shows the S_{11} response of the CP antenna with different array dimensions for the FSS that is used as a superstrate over the radiating patch. Axial ratio and gain variation of the CP antenna loaded with FSS for different array sizes are shown in Fig. 17.

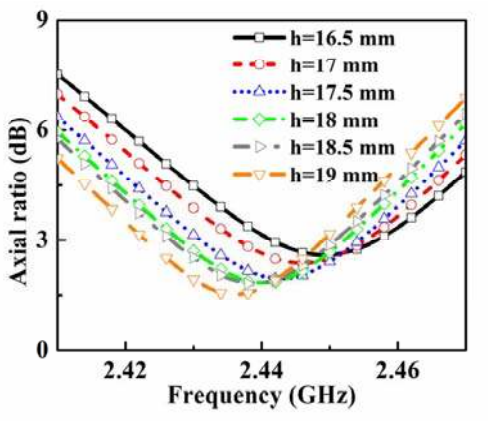

Figure 13. Changes in axial ratio for different positions of the FSS above patch.

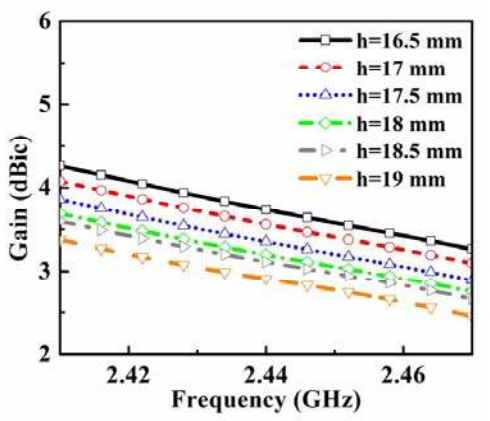

Figure 14. Changes in gain for different positions of the FSS above patch.

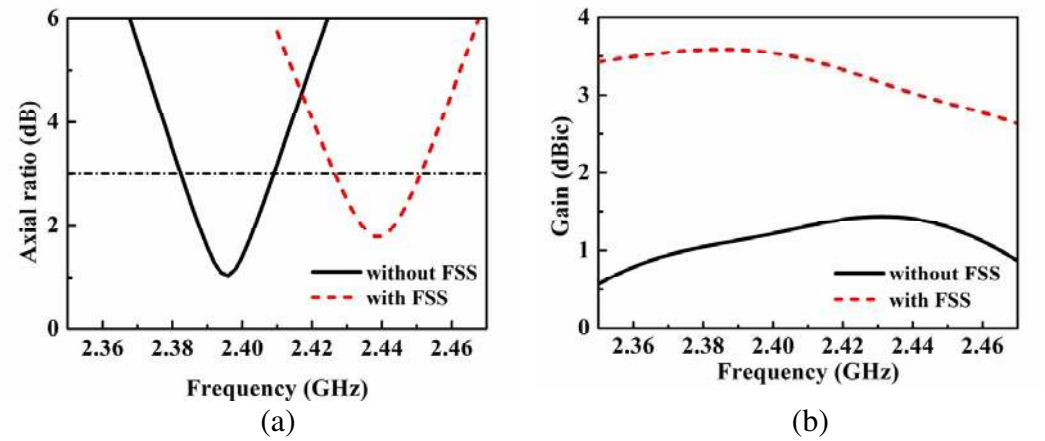

Figure 15. Simulated (a) axial ratio and (b) gain variation of the antenna with and without FSS.

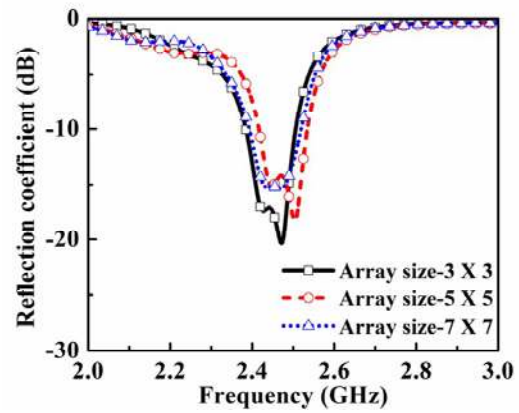

Figure 16. Simulated reflection coefficient plot for different FSS array size.

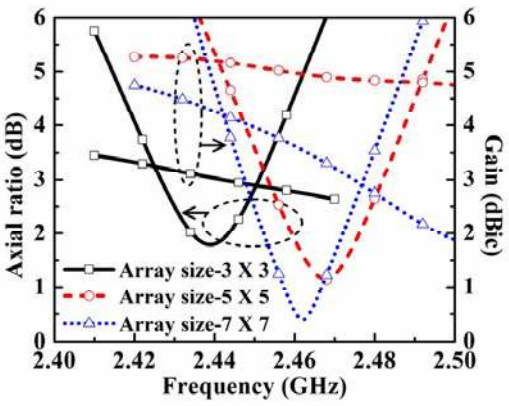

Figure 17. Simulated axial ratio and gain plot for different FSS array size.

Table 1. Characteristics of the antenna without and with FSS.

Antenna	Operating frequency	Impedance bandwidth	Axial ratio bandwidth	Gain	Radiation efficiency
Without FSS	2.4 GHz	2.346–2.461 GHz (115 MHz or 4.78%)	2.382–2.409 GHz (27 MHz or 1.13%)	1.22 dBi	32%
With FSS	2.45 GHz	2.385–2.506 GHz (121 MHz or 4.95%)	2.426–2.451 GHz (25 MHz or 1.03%)	3.03 dBi	42%

6. MEASURED RESULTS

The prototype of the proposed antenna is fabricated and measured to validate the simulated results. A photograph of the fabricated antenna is shown in Fig. 18. Plastic spacers are used to support the FSS above the antenna at a height of 18.3 mm from radiating patch surface. Reflection coefficients of the antenna without and with FSS are measured using Keysight N5224B microwave network analyzer, and

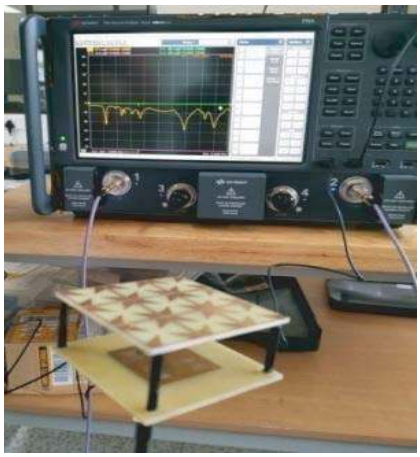

Figure 18. Photograph of the fabricated antenna with FSS.

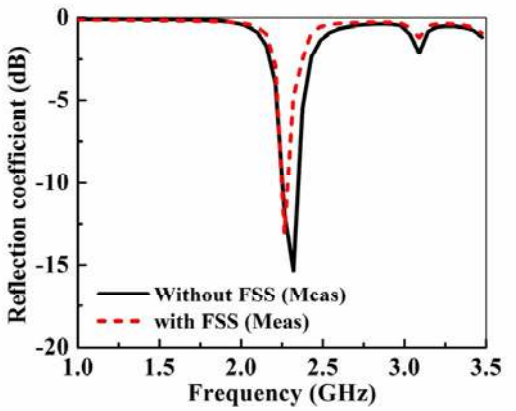

Figure 19. Measured reflection coefficient of the antenna with and without FSS.

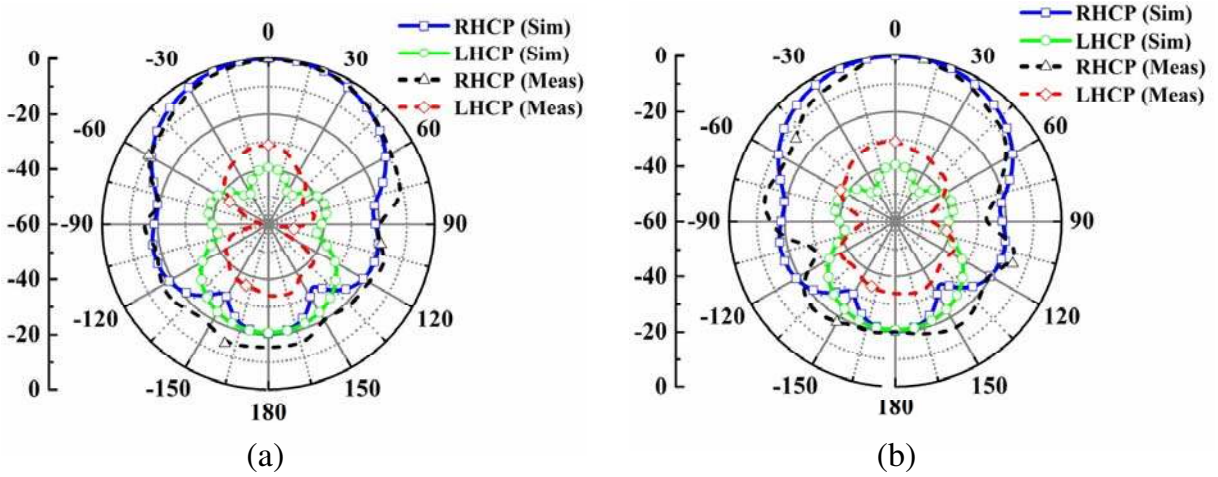

Figure 20. Simulated and measured radiation pattern of the proposed antenna with FSS in (a) XZ plane, (b) YZ plane.

measured reflection coefficient plots are shown in Fig. 19.

Measured impedance bandwidth of the proposed FSS loaded CP antenna is 122 MHz (2.248–2.37 GHz) which is very close to simulated bandwidth of 121 MHz (2.385–2.506 GHz). The shift in center frequency in the impedance bandwidth as compared to simulated results occurs due to fabrication tolerance and variation of dielectric constant of the substrate. The radiation patterns of the composite antenna structure are measured at two planes XZ ($\Phi = 0°$) and YZ ($\Phi = 90°$), and it is shown in Fig. 20 along with simulated radiation patterns. Small deviation between simulated and measured radiation patterns occurs which may be due to an improper measurement setup and the effect of plastic spacers. The measured gain of the antenna is 2.7 dBic at operating frequency which is slightly lower than the simulated gain of 3.02 dBic.

Table 2. Comparison of this work with other CP antennas in previous literature.

Ref.	Frequency	Techniques	Imp. BW	AR BW	Peak Gain	Patch Size	Substrate
[10]	2.4 GHz	Asymmetric slits	2.5%	0.5%	4.3 dBic	$0.253\lambda_0 \times 0.253\lambda_0$	RO4003C ($\varepsilon_r = 3.38$)
[15]	2.4 GHz	Symmetric CSRRs	4.8%	1.11%	0.62 dBic	$0.204\lambda_0 \times 0.196\lambda_0$	FR4 ($\varepsilon_r = 4.4$)
This work	2.4 GHz	Asymmetric CSRRs	4.8%	1.13%	1.22 dBic	$0.205\lambda_0 \times 0.202\lambda_0$	FR4 ($\varepsilon_r = 4.4$)
[13]	2.824 GHz	CSRRs with RIS	4.9%	1.68%	NA	$0.186\lambda_0 \times 0.186\lambda_0$	MEGTRON 6 (($\varepsilon_r = 4.02$)
[17]	2.86 GHz	Meta-resonators with RIS	1.75%	1.05%	4.15 dBic	$0.248\lambda_0 \times 0.248\lambda_0$	F4B ($\varepsilon_r = 2.65$)
This work	2.44 GHz	CSRRs with FSS	4.95%	1.03%	3.23 dBic	$0.205\lambda_0 \times 0.202\lambda_0$	FR4 ($\varepsilon_r = 4.4$)

7. CONCLUSION

A comparison of this work with other similar works for CP antennas operating between 2 and 3 GHz is shown in Table 2. Though the gain of the proposed antenna is not improved as compared to [10] and [17], there is a considerable improvement in impedance bandwidth and miniaturization of the antenna. The advantage of this work is that this antenna is made on a commercially available low cost FR4 substrate. In this paper, a compact and low profile circularly polarized antenna based on four asymmetric CSRRs loaded along the diagonal direction is presented. Further to improve the radiation efficiency and gain of the antenna a 3×3 FSS superstrate is placed at a height of 18.3 mm from the radiating patch. The overall profile of the antenna is approximately $\lambda/8$ which is smaller than the conventional $\lambda/2$ thickness for FP cavity antenna. The simulated 10 dB impedance bandwidth and 3 dB axial ratio bandwidth of the composite antenna structure are 4.95% and 1.03%, respectively. Measured impedance bandwidth is 5.28% which is slightly higher than the simulated one. At the operating frequency, simulated and measured gains of the antenna are 3.02 dBic and 2.7 dBic, respectively. The proposed FSS loaded CP antenna exhibits right-handed polarization (RHCP), and its measured and simulated radiation patterns exhibit broadside radiation property.

ACKNOWLEDGMENT

Authors acknowledge Prof. Bhaskar Gupta, Jadavpur University and Dr. Sukomal Dey, IIT Palakkad for providing the facility for measurement of the device. Authors also acknowledge the reviewers for their valuable comments and suggestions for improvement of this work.

REFERENCES

1. Balanis, C. A., "Antenna theory: A review," *Proceedings of the IEEE*, Vol. 80, No. 1, 7–23, 1992.
2. Kumar, G. and K. P. Ray, *Broadband Microstrip Antennas*, Artech House, 2003.
3. Sharma, P. C. and K. C. Gupta, "Analysis and optimized design of single feed circularly polarized microstrip antennas," *IEEE Trans. Antennas Propag.*, Vol. 31, No. 6, 949–955, 1983.
4. Iwasaki, H., "A circularly polarized small-size microstrip antenna with a cross slot," *IEEE Trans. Antennas Propag.*, Vol. 44, No. 10, 1399–1401, 1996.
5. Yang, K. P., K. L. Wong, and J. Lu, "Compact circularly polarized triangular microstrip antenna with y-shaped slot," *Microw. Opt. Technol. Lett.*, Vol. 20, No. 1, 31–34, 1999.
6. Sharma, W. C., H. Kumar, and G. Kumar, "Single feed dual band circularly polarized stub loaded tunable microstrip patch antenna," *IEEE Asia-Pacific Microwave Conference (APMC)*, 2016.
7. Chen, W. S., C. K. Wu, and K. L. Wong, "Single-feed square-ring microstrip antenna with truncated corners for compact circular polarisation operation," *Electronics Letters*, Vol. 34, No. 11, 1045–1047, 1998.
8. Nasimuddin, Z. N. Chen, and X. Qing, "Asymmetric-circular shaped slotted microstrip antennas for circular polarization and RFID applications," *IEEE Trans. Antennas Propag.*, Vol. 58, No. 12, 3821–3828, 2010.
9. Chen, Z. N. and X. Qing, "Compact circularly polarized asymmetric-slotted microstrip patch antennas," *Microw. Opt. Technol. Lett.*, Vol. 54, No. 8, 1920–1927, 2012.
10. Qing, X. and Z. N. Chen, "Compact asymmetric-slit microstrip antennas for circular polarization," *IEEE Trans. Antennas Propag.*, Vol. 59, No. 1, 285–288, 2011.
11. Caloz, C. and T. Itoh, *Electromagnetic Metamaterials: Transmission Line Theory and Microwave Applications*, Wiley-Interscience, 2006.
12. Liu, X. Y., Z. T. Wu, Y. Fan, and E. M. Tentzeris, "A miniaturized CSRR loaded wide-beamwidth circularly polarized implantable antenna for subcutaneous real-time glucose monitoring," *IEEE Antennas Wireless Propag. Lett.*, Vol. 16, 577–580, 2017.
13. Dong, Y., H. Toyao, and T. Itoh, "Design and characterization of miniaturized patch antennas loaded with complementary split-ring resonators," *IEEE Trans. Antennas Propag.*, Vol. 60, No. 2, 772–785, 2012.
14. Ke, L., G.-M. Wang, X. Tong, and H.-X. Xu, "A novel circularly polarized antenna based on the single complementary split ring resonator," *IEEE International Symposium on Signals, Systems and Electronics*, 2010.
15. Dey, S., S. Mondal, and P. P. Sarkar, "Single feed circularly polarized antenna loaded with complementary split ring resonator (CSRR)," *Progress In Electromagnetics Research M*, Vol. 78, 175–184, 2019.
16. Dey, S., S. Mondal, and P. P. Sarkar, "Reactive impedance surface (RIS) based asymmetric slit patch antenna loaded with complementary split ring resonator (CSRR) for circular polarization," *Journal of Electromagnetic Waves and Applications*, Vol. 33, No. 8, 1003–1013, 2019.
17. Xu, H. X., G. M. Wang, J. G. Liang, M. Q. Qi, and X. Gao, "Compact circularly polarized antennas combining meta-surfaces and strong space-filling meta-resonators," *IEEE Trans. Antennas Propag.*, Vol. 61, No. 7, 3442–3450, 2013.
18. Wang, Y., et al., "Planar vortex beam generator for circularly polarized incidence based on FSS," *IEEE Trans. Antennas Propag.*, Vol. 68, No. 3, 1514–1522, 2019.
19. Foroozesh, A. and L. Shafai, "Investigation into the effects of the patch-type FSS superstrate on the high-gain cavity resonance antenna design," *IEEE Trans. Antennas Propag.*, Vol. 58, No. 2, 258–270, 2010.
20. Liu, Z. G., Z. X. Cao, and L. N. Wu, "Compact low-profile circularly polarized Fabry-Perot resonator antenna fed by linearly polarized microstrip patch," *IEEE Antennas Wireless Propag. Lett.*, Vol. 15, 524–527, 2015.

21. Lee, D. H., Y. J. Lee, J. Yeo, R. Mittra, and W. S. Park, "Directivity enhancement of circular polarized patch antenna using ring-shaped frequency selective surface superstrate," *Microw. Opt. Technol. Lett.*, Vol. 49, No. 1, 199–201, 2007.
22. Chatterjee, A. and S. K. Parui, "A dual layer frequency selective surface reflector for wideband applications," *Radio Engineering*, Vol. 25, No. 1, 2016.
23. CST Microwave Studio Manual, ver. 14, Computer Simulation Technology, Framingham, MA.